HHS Public Access

Author manuscript

Health Phys. Author manuscript; available in PMC 2017 November 28.

Published in final edited form as:

Health Phys. 2016 December ; 111(6): 542–558. doi:10.1097/HP.0000000000000572.

USE OF TRANSPORTABLE RADIATION DETECTION INSTRUMENTS TO ASSESS INTERNAL CONTAMINATION FROM INTAKES OF RADIONUCLIDES PART II: CALIBRATION FACTORS AND ICAT COMPUTER PROGRAM

Robert Anigstein[*], **Richard H. Olsher**[†], **Donald A. Loomis**[*], and **Armin Ansari**[‡]

[*]S. Cohen & Associates, 1608 Spring Hill Road, Vienna, VA 2218

[†]HP Consulting, LLC, 20 Grand Canyon Drive, Los Alamos, NM 87544

[‡]Radiation Studies Branch, EHHE, NCEH, Centers for Disease Control and Prevention; Atlanta, GA 30341-3717

Abstract

The detonation of a radiological dispersion device or other radiological incidents could result in widespread releases of radioactive materials and intakes of radionuclides by affected individuals. Transportable radiation monitoring instruments could be used to measure radiation from gamma-emitting radionuclides in the body for triaging individuals and assigning priorities to their bioassay samples for in vitro assessments. The present study derived sets of calibration factors for four instruments: the Ludlum Model 44-2 gamma scintillator, a survey meter containing a 2.54 × 2.54-cm NaI(Tl) crystal; the Captus 3000 thyroid uptake probe, which contains a 5.08 × 5.08-cm NaI(Tl) crystal; the Transportable Portal Monitor Model TPM-903B, which contains two 3.81 × 7.62 × 182.9-cm polyvinyltoluene plastic scintillators; and a generic instrument, such as an ionization chamber, that measures exposure rates. The calibration factors enable these instruments to be used for assessing inhaled or ingested intakes of any of four radionuclides: ^{60}Co, ^{131}I, ^{137}Cs, and ^{192}Ir. The derivations used biokinetic models embodied in the DCAL computer software system developed by the Oak Ridge National Laboratory and Monte Carlo simulations using the MCNPX radiation transport code. The three physical instruments were represented by MCNP models that were developed previously. The affected individuals comprised children of five ages who were represented by the revised Oak Ridge National Laboratory pediatric phantoms, and adult men and adult women represented by the Adult Reference Computational Phantoms described in Publication 110 of the International Commission on Radiological Protection. These calibration factors can be used to calculate intakes; the intakes can be converted to committed doses by the use of tabulated dose coefficients. These calibration factors also constitute input data to the ICAT computer program, an interactive Microsoft Windows-based software package that estimates intakes of radionuclides and cumulative and committed effective doses, based on

For correspondence contact: Robert Anigstein, S. Cohen & Associates, 740 West End Avenue, Apt. 95A, New York, NY 10025, or anigstein@cs.com.

The authors declare no conflicts of interest.

measurements made with these instruments. This program constitutes a convenient tool for assessing intakes and doses without consulting tabulated calibration factors and dose coefficients.

Keywords

biokinetics; detector; scintillation; intake; radionuclide; phantom mathematical

INTRODUCTION

Following a radiological emergency, such as the detonation of a radiological dispersion device (RDD or “dirty bomb”), a severe reactor accident, or the surreptitious introduction of radioactive materials into food or drinking water, a large number of people could suffer internal contamination. Intakes of radioactive materials could be assessed in the field by means of in vivo bioassay, using radiation detection instruments to measure external gamma radiation from radionuclides in the body. Such assessments could be used for field triage: to identify and assign priorities to those individuals requiring medical follow-up. They could also provide reassurance to potentially contaminated individuals who have not, in fact, taken in significant amounts of radioactive materials.

In vivo bioassay is not a new concept. The nuclear weapons complex has used whole-body counters employing large-volume NaI(Tl) detectors to measure body burdens since the mid-1950s. These counters were calibrated with anthropomorphic phantoms and human volunteers. Chest counters for $^{239/240}$Pu and ^{241}Am were introduced in the mid-1960s. Whole-body counters are used widely in commercial nuclear power plants. However, such counters are few in number and not readily transportable; they would be of limited use in assessing a large number of potentially affected individuals in a radiological emergency. On the other hand, portable or transportable radiation monitoring instruments are widely available. However, calibration factors are required to use readings on such instruments to estimate intakes of radionuclides and cumulative and committed doses.

Previous studies

Several studies have aimed to develop relationships between count rates and radionuclide distributions in the human body that would enable the use of radiation detection and measuring instruments to assess internal contamination of individuals following intakes of radioactive materials.

Kramer et al. (2005) used a high-purity germanium detector coupled to a multichannel analyzer (MCA) to measure count rates from aqueous solutions of radionuclides contained in hollow compartments of the Bottle Manikin Absorber (BOMAB) phantom representing a reference adult male, described by Kramer et al. (1991). Kramer et al. (2005) used a model of the detector constructed with the MCNP5 (Monte Carlo N-Particle, Version 5) radiation transport computer code to simulate the counting efficiencies of the detector when exposed to photons spaning a range of energies emitted by radiation sources in six members of the BOMAB phantom family. These comprised two children (4- and 10-y-old); 5th percentile, reference, and 95th percentile adult males; and a reference adult female. They used these

simulations to develop an analytical expression to predict the counting efficiency of the instrument as a function of photon energy and the weight:height ratio of the individual. This expression was to be used to estimate the body burden of a given radionuclide, assuming a uniform distribution in the whole body. That result was then to be used as input to a biokinetic model to estimate intake and dose.

Anigstein et al. (2007–2010) developed calibration factors to enable nuclear medicine gamma cameras to be used for assessing intakes of radionuclides. The study used biokinetic models embodied in the Oak Ridge National Laboratory (ORNL) DCAL computer program (described later in the present paper) to determine the retention of radio-nuclides taken into the body and their distribution among selected anatomical regions as a function of time following intake. Normalized count rates from activities of six radionuclides —^{60}Co, ^{90}Sr, ^{131}I, ^{137}Cs, ^{192}Ir, and ^{241}Am—in selected anatomical regions of children of five ages and in an adult male and an adult female were calculated using the MCNPX (Monte Carlo N-Particle eXtended) radiation transport code. Children were represented by pediatric phantoms in the revised ORNL phantom series described by Han et al. (2006), while the adult male and adult female were represented by the NORMAN and NAOMI voxel phantoms (Dimbylow 1998, 2005). These calibration factors were incorporated into Assess, a Microsoft Windows-based interactive computer program that uses count rates on gamma cameras to calculate the inhaled or ingested intake of any of the six radionuclides, the committed effective dose, and the cumulative effective dose delivered up to the time of the assessment (Anigstein et al. 2009).

Manger et al. (2012) used MCNP5 and biokinetic models to simulate the responses of two plastic scintillation detectors to inhaled intakes of ^{60}Co, ^{131}I, ^{137}Cs, and ^{192}Ir by a reference adult male who was represented by a stylized anthropomorphic phantom described by Eckerman et al. (1996). The authors reported count rates as a function of time after an intake that would deliver a dose of 250 mSv CEDE.

Palmer et al. (2012) used MCNP5 and biokinetic models to simulate the response of the Transportable Portal Monitor Model TPM-903B (manufactured by Rapiscan Systems, Longmont, CO, USA, and distributed by Thermo Fisher Scientific Inc., Franklin, MA, USA) to inhaled and ingested intakes of ^{60}Co, ^{131}I, ^{137}Cs, and ^{192}Ir by reference and adipose adult males and adult females, a postmenopausal adipose female, and a 10-y-old child. The adults were represented by stylized anthropomorphic phantoms based on the reference male phantom developed at ORNL, with additions of adipose tissue to represent adipose individuals. The child was represented by an anthropomorphic phantom constructed using the BodyBuilder computer program (White Rock Science, Los Alamos, NM, USA). The authors reported count rates as a function of time after intakes that would deliver a committed effective dose of 10 mSv.

Bolch et al. (2012) used MCNPX and biokinetic models to simulate the response of four survey meters—three using NaI(Tl) detectors and one using a GM pancake probe—to radionuclides inhaled or ingested by a reference adult male and adult female, represented by voxelized hybrid computational phantoms described by Hurtado et al. (2012). Bolch et al. reported count rates as a function of time after intakes of five radionuclides

—^{60}Co, ^{131}I, ^{137}Cs, ^{192}Ir, and ^{241}Am—that would deliver committed effective doses of 50, 250, or 500 mSv. Each instrument was in one of four positions and at one of four distances with respect to the body.

Dewji et al. (2013) used MCNP5 and biokinetic models to simulate the response of a monitor employing a 5.08 × 5.08-cm NaI(Tl) detector and an MCA to radionuclides inhaled by reference and adipose adult males and adult females, a postmenopausal adipose female, and a 10-y-old child. The adults were represented by stylized anthropomorphic phantoms based on the reference male phantom described by Eckerman et al. (1996), with additions of skin and adipose tissue to represent adipose individuals. The child was represented by an anthropomorphic phantom constructed using the BodyBuilder computer program. The authors reported count rates as a function of time after an intake of each of five radionuclides —^{60}Co, ^{131}I, ^{137}Cs, ^{192}Ir, and ^{241}Am—that would deliver a committed effective dose of 250 mSv.

Present work

The present paper is the second of a two-part series. In Part I, Anigstein et al. (2016) measured count rates from calibrated sources of ^{60}Co, ^{137}Cs, and ^{241}Am on three instruments:

1. Ludlum Model 44-2 sodium iodide (NaI[Tl]) gamma scintillator (Ludlum Measurements Inc., Sweetwater, TX, USA), a survey meter containing a 2.54 × 2.54-cm NaI(Tl) crystal;
2. Captus 3000 thyroid uptake probe (Capintec Inc., Sales and Marketing and Customer Support, Ramsey, NJ, USA), which contains a 5.08 × 5.08-cm NaI(Tl) crystal; and
3. Transportable Portal Monitor Model TPM-903B, which contains two 3.81 × 7.62 × 182.9-cm polyvinyltoluene plastic scintillators.

Computer models were constructed of the instruments and of the calibration sources, using engineering drawings and other data provided by the manufacturers; count rates from these sources were simulated by MCNPX. The count rates derived from the computer simulations were within ±16% of the measured count rates for all 20 measurements, without the use of empirical radionuclide-dependent scaling factors employed by other authors. The weighted root-mean-square deviations (differences between measured and simulated count rates, added in quadrature and weighted by the variance of the difference) were 10.9% for the survey meter, 4.2% for the thyroid probe, and 0.9% for the portal monitor. These results validated the MCNP[1] models of these instruments.

The present study developed calibration factors to enable the use of these instruments to estimate intakes of four gamma-emitting radionuclides—^{60}Co, ^{131}I, ^{137}Cs, and ^{192}Ir—which in turn can be used to estimate committed doses. Cobalt-60, ^{137}Cs, and ^{192}Ir were selected

[1]The term “MCNP” refers to a family of codes which includes MCNP5, MCNPX, and MCNP6. In the present report, the term “MCNPX” is used to refer to the use of that specific code and to features that are unique to that code; the generic term “MCNP” is used to describe features and capabilities common to the MCNP family.

from among the “nine isotopes of interest for RDDs” listed by ANL (2007), eight of which are also listed among the “isotopes of greatest concern” by DOE/NRC (2003). These radionuclides are widely used in medical and industrial applications and can be readily detected and measured by the field instruments included in the present study. The remaining five radionuclides common to both lists include ^{90}Sr, a beta emitter, which is addressed in the discussion section of the present paper, and ^{210}Po, ^{238}Pu, and ^{241}Am, which decay by alpha emission. The object of the present study is to facilitate the assessment of internal contamination at levels below the Clinical Decision Guide (CDG) defined by NCRP (2008).[2] The high radiotoxicity of these three radionuclides, combined with their low detectability, precludes their being detected at CDG levels by the field instruments used in the present study.[3] The last of the five radionuclides, ^{252}Cf, is an alpha emitter that undergoes spontaneous fission in 3.1% of its disintegrations. Because of its limited availability and because its emission spectra change with the ingrowth of fission products, requiring calibration factors that depend on the age of the material, it was not included in the present study.

Iodine-131 was included because it is a major potential constituent of radioactive releases following a nuclear reactor accident. It was the only radionuclide released in significant quantities following the Three Mile Island accident, other than radioactive noble gases that are not retained in the body (Behling and Hildebrand 1986).

MATERIALS AND METHODS

Calibration factors for assessment of intakes

Using a radiation detector to assess the intake of a radionuclide requires a set of calibration factors that relate the inhaled or ingested activity to the count rate or exposure rate registered on the instrument. Such factors depend on the distribution of activity in the body at the time of assessment and vary with the age and gender of the individual. They also depend on the model of the instrument and on the energy window (if any) used for the measurement.

The derivation of these calibration factors proceeds in a series of three steps:

1. Use of biokinetic models to determine the fraction of the activity in each anatomical region as a function of time after intake. The fraction will depend on: (a) mode of intake (inhalation or ingestion), (b) elapsed time following intake, (c) particle size distribution (for intake by inhalation), (d) lung absorption type of the radionuclide (for intake by inhalation), and (e) age of individual;
2. Use of Monte Carlo simulations to determine the count rate on a given instrument or the exposure rate, normalized to a unit activity in each anatomical region. The rate will depend on: (a) model of instrument, (b) position of

[2]The CDG, as defined by NCRP (2008), specifies a limit of 250 mSv for consideration of stochastic effects on adults but also includes limits on doses to the lungs and to bone marrow, and different limits for radioiodines, for children up to 18-y-old, and for pregnant women.

[3]Anigstein et al. (2007–2010) found that gamma cameras can be used to detect internal contamination with ^{241}Am at levels below the CDG under favorable circumstances.

instrument with respect to the body, (c) energy window (if applicable), and (d) age (of child) or gender (of adult); and

3. Calculating the intake activity corresponding to a nominal rate of 1 min^{-1} or 7.17 × 10^{-14} C kg^{-1} s^{-1}.

Biokinetic models

Biokinetic modeling was performed using the DCAL (Dose and Risk Calculation) computer software package (ORNL 2006), "a comprehensive software system for the calculation of tissue dose and subsequent health risk from intakes of radionuclides or exposure to radionuclides present in environmental media" (Eckerman et al. 2006). DCAL calculates the activities of radionuclides in selected anatomical regions (referred to as "source regions") of reference individuals of specified ages at times ranging from approximately 1 min up to 100 y after intake. DCAL was used to determine the distribution of activities in the source regions over a range of time following the acute intake of a unit activity of each of the radionuclides included in the present study.

DCAL parameters—The present study assessed individuals at six stages of development —infant (age 100 days); ages 1, 5, 10, and 15 y; and adult (age ≥20 y for elements represented by the radionuclides in the present study)—that correspond to the age-specific biokinetic models used by ICRP (1996). Fifty time steps, spaced logarithmically over the interval 1 h–30 d following intake, were selected for calculating activity distributions used by the ICAT computer program (Anigstein et al. 2014). The time steps start at 1 h because that is the minimum likely time for the affected individual to undergo external decontamination and be assessed with a field instrument.

The radionuclides included in the study are isotopes of four chemical elements. All lung absorption types of these elements that are listed by ICRP (2012, Table E.1) are represented in the calibration factors for inhalation. These absorption types, which apply to inhaled particulate matter in the workplace, were used in the absence of guidance on chemical forms of radionuclides that would be released in a radiological emergency. It is likely that these forms would fall into the wide classes of compounds generated in industrial workplaces. These lung absorption types are listed in Table 1.

The size distribution of inhaled particles was based on data presented by Harper et al. (2007), who investigated the distribution of aerosols following the detonation of a simulated RDD. The aerosols comprised a wide range of particle sizes; however, measurements performed during these experiments indicated that individuals in the vicinity of the detonation would be exposed to the inhalation of particles with a characteristic size on the order of 1 μm aerodynamic equivalent diameter. The further the exposed individual would be from the site of the detonation, the smaller the particle size of the inhaled intake. Based on these results, the present analyses assumed a particle size distribution of 1 μm activity median aerodynamic diameter (AMAD) in deriving calibration factors for inhalation.

The derivation of the calibration factors employed the age-dependent f_1 values used in deriving the risk coefficients listed in Federal Guidance Report No. 13 (Eckerman et al. 1999) that are furnished with DCAL and are listed in Table 2.

DCAL calculates the distribution of a given radionuclide among as many as 57 source regions, depending on the biokinetic model of the chemical element. For each radionuclide, a set of source regions was selected that contains at least 99% of the total activity retained in the body at any time from 1 h to 30 d after intake—these regions are listed in Table 3. The distributions of four radionuclides in the source regions of reference individuals at six different stages of development at 12 times after intake are tabulated by Anigstein and Olsher (2016, Appendix B). These time steps are a subset of the 50 time steps used by ICAT.

MCNPX simulation of count rates

MCNPX was used to simulate the responses of three physical instruments to distributions of four radionuclides in anatomical regions of children of five ages and adults of both genders. The analysis combined MCNP models of these instruments with five pediatric and two adult computational phantoms. In addition to simulating count rates on physical detectors, MCNPX was used to simulate exposure rates at various locations outside the phantoms. The results of these analyses are sets of empirical relationships between the count rates on each instrument (and the exposure rates that constitute a virtual instrument) and activities in a given anatomical region.

MCNP models of pediatric phantoms

Eckerman et al. (1996) described a series of anthropomorphic phantoms representing individuals at different stages of development, from infant to adult, developed at ORNL. Han et al. (2006) described revisions to the ORNL phantom series that incorporate later developments in the field, including the anatomical data presented by ICRP (2002). The MCNP pediatric models that are based on these revised phantoms were furnished to the present authors by Prof. Wesley Bolch.[4] These models include both male and female organs. In the case of the 15-y-old phantom, its total mass—approximately 57 kg—is greater than the 56-kg mass of the 15-y-old reference male, which is greater than the 53-kg mass of the 15-y-old reference female (ICRP 2002, Table 2.8). These phantoms were therefore used to represent male individuals; female breasts and reproductive organs were eliminated from the models. However, the results of the simulations are also applicable to females. In the case of 15-y-olds, the variability among real individuals overshadows the anatomical differences between the reference male and the reference female.

For the purpose of the present analysis, it was necessary to establish a correspondence between the anatomical regions of the revised ORNL phantoms and the DCAL source regions. As shown in Table 4, the bronchial mucosa, one of the anatomical regions of the revised ORNL phantoms, corresponds to three source regions in the DCAL model. The sum of the activities in these source regions was assigned to the corresponding phantom region.

[4]Wesley E. Bolch, Director, Advanced Laboratory for Radiation Dosimetry Studies (ALRADS), Department of Nuclear and Radiological Engineering, University of Florida, 6 October 2005, personal e-mail to Richard H. Olsher.

Conversely, the source regions comprising the contents of the upper and lower large intestines and the kidneys each correspond to more than one anatomical region in the phantoms. The activity in each such source region was distributed among the corresponding anatomical regions in proportion to the mass of each anatomical region in each phantom, as listed by Han et al. (2006, Tables 5 and 6), resulting in equal concentrations in these regions.[5] Finally, the lungs of the phantoms correspond to four DCAL source regions. The total activity in these source regions was distributed among the two lungs in proportion to the mass of each lung. The relative masses of each of these phantom regions are listed in Table 4 for each of the five pediatric phantoms. Regions for which there is an obvious 1:1 correspondence between the phantoms and the DCAL models are not listed.

The revised ORNL phantoms do not have a single region that contains the total volume of blood in the body, a DCAL source region. A blood region was created in each pediatric phantom by combining the blood contents of each anatomical region. (These regions include the contents of the heart, which comprises 9% of the total blood volume in adults.) Absent comparable data for children, the distribution of regional blood volumes in adult males, listed by ICRP (2002, Table 2.14), was used to calculate the blood content of each phantom region.[6] If a region in the ICRP blood volume distribution corresponds to more than one phantom region, the activity in that blood region was distributed among those phantom regions in proportion to the mass of each phantom region. The percentage of the total blood volume assigned to each region of each of the five revised ORNL pediatric phantoms is listed by Anigstein and Olsher (2016, Appendix A, Table A-1). The blood region in each phantom comprises a set of anatomical regions that contain at least 99% of the blood in the body.

The biokinetic models of cobalt, iodine, and iridium include a source region described as *Other*. This region comprises all tissues other than those explicitly specified in the biokinetic model of the given element, excluding body fluids and the contents of lumina.[7] Thus, the tissues comprising this region depend on the particular element being modeled. The activity in the *Other* region—calculated by DCAL—was distributed among the anatomical regions of the revised ORNL phantoms comprising the *Other* region in proportion to the mass of each phantom region. The percent activity in each anatomical region is listed by Anigstein and Olsher (2016, Appendix A, Tables A-2 to A-4). The biokinetic model of cesium includes a region called *Body Tissues* that comprises all living tissues not otherwise included in the model, excluding mineralized bone. The calculated activity in *Body Tissues* was distributed among the corresponding anatomical regions in the revised ORNL phantoms in the same manner as the distribution of the *Other* activity. The percent activities in the anatomical regions comprising *Body Tissues* are listed by Anigstein and Olsher (2016, Appendix A, Table A-5). As was the case for the blood region, the selected sets of

[5]The mass of each anatomical region depends on the age of the reference individual. Thus, the relative activities in the anatomical regions corresponding to a given source region will vary with age; however, the activity concentration in each of the anatomical regions corresponding to a given source region in a given phantom will be uniform.

[6]The only significant difference between the reference values of distribution of blood volumes in adult males and adult females is the relative proportion of blood in muscle and in fat. The distribution for the adult male was used because the average ratio of muscle to fat in children (newborn to age 15 y) is closer to the muscle-to-fat ratio in adult males than in adult females.

[7]Keith Eckerman, Oak Ridge National Laboratory, April 2007, private communication with Robert Anigstein.

anatomical regions comprise 99% of the total mass of the *Other* and *Body Tissues* regions of each phantom.

MCNP models of adults—The MCNP models of adults are based on the Reference Male and Female Computational Phantoms (RMCP and RFCP) described by ICRP (2009). These voxel phantoms were created from MRI images of an adult male and adult female, each of whose height and mass were scaled to the corresponding ICRP reference values (ICRP 2002, Table 2.8). Each phantom is composed of 141 anatomical regions. Each of these regions is composed of one of 53 media (teeth, mineral bone, etc.). The density and elemental composition of each medium in the RMCP and RFCP are listed by ICRP (2009, Annex B).

Relationships were established between the DCAL source regions and the corresponding anatomical regions in the RMCP and RFCP, as shown in Table 5. The first column in this table displays the names of the anatomical regions, as listed by ICRP (2009, Table A.1), that are grouped to correspond to the DCAL source regions listed in the last column. The sum of the activities in the DCAL regions was distributed among the corresponding voxel regions in proportion to the relative masses of these voxel regions, as listed by ICRP (2009; Table A.1). Regions for which there is an obvious 1:1 correspondence between the voxel phantoms and the DCAL models are not shown in Table 5.

Neither the RMCP nor the RFCP has a single region that contains the total blood volume. It was therefore necessary to specify the regions of the voxel phantoms that comprise the DCAL blood region. These phantoms do include major blood vessels in the head, trunk, arms, and legs. They also include regions identified as “Heart contents (blood)” and blood in the left and right lungs. However, these regions constitute only a fraction of the total blood in the body. In the case of the RMCP, for example, the total mass of these regions is 1,032 g, compared to a mass of 5,600 g of blood in the reference adult male (ICRP 2002, Table 2.8). A comparable situation is found in the RFCP. The reason for these discrepancies is that small vessels and capillaries could not be segmented in the MRI images that have a resolution of ~2 mm in the horizontal planes of both phantoms, 8 mm in the vertical direction in the RMCP, and 5 mm in the RFCP. ICRP (2009) accounted for the blood content of the other organs and tissues by including it in the elemental composition of the corresponding media. This was accomplished by combining the elemental composition of the organ parenchyma with the elemental composition of blood, adjusted for the fraction of blood in that organ or tissue.

In the present analysis, DCAL blood regions were constructed for the RMCP and the RFCP by combing the blood in each of the 141 regions in each phantom that contained significant amounts of blood. The mass of blood in each voxel region was calculated by multiplying the total mass of that region by the blood fraction of the medium constituting that region, as listed by ICRP (2009, CD 4). These blood regions comprise the blood contents of 77 voxel regions in the RMCP and 78 regions in the RFCP. Each blood region contains 99% of the total blood in the respective phantom. [The percentage of the total blood in each constituent region is listed by Anigstein and Olsher (2016, Appendix A, Table A-6).] The remaining 1% of the blood is distributed among the listed voxel regions.

The construction of the DCAL *Other* and *Body Tissues* regions in the RMCP and RFCP was performed in a manner similar to the construction of these regions in the revised ORNL pediatric phantoms. The percent activities of each of the four radionuclides in each anatomical region of the RMCP and RFCP that is a component of the *Other* or *Body Tissues* regions are listed by Anigstein and Olsher (2016, Appendix A, Table A-7).

Exposure geometries—As stated earlier, the MCNPX simulations used computer models of three instruments—the Ludlum Model 44-2 gamma scintillator, the Captus 3000 thyroid uptake probe, and the Model TPM-903B portal monitor—to construct the exposure geometries used in the present study. These geometries combined the models of these instruments with the MCNP models of the five pediatric and two adult anthropomorphic phantoms discussed above. The instrument models include two versions of the TPM-903B: the standard model that has a 32-inch (81.28-cm) separation between the columns, and the extra-wide model used by the State of Georgia.

The geometries for the Ludlum and Captus detectors include 9 to 10 positions with respect to each phantom. With both instruments, the probes are in contact with the skin and at a distance of 30.48 cm in the anteroposterior (AP) and posteroanterior (PA) orientations, centered on the phantom. The cylindrical axis of each probe lies in a horizontal plane that passes through the center of mass of the lungs or the center of mass of the stomach. The lung positions are used for simulating count rates from inhaled intakes and the stomach positions for ingested intakes. Fig. 1 shows a cross-section in the midsagittal plane of the 1-y-old phantom with the Ludlum probe proximal to the lungs, produced by MCNPX, while Fig. 2 is a corresponding illustration of the 10-y-old with the Captus probe proximal to the stomach. The stomach lies to the left of the midsagittal plane in this stylized phantom and therefore does not appear in this view. Only the proximal positions of the instruments are shown; in the distal positions, the instrument is translated away from the body along its horizontal axis.

Additional simulations were performed of count rates on detectors anterior to the thyroid following intakes of ^{131}I. The probes were positioned at the closest distance to the thyroid, and also at a distance of 30.48 cm (1 foot) anterior to the neck. The exception was the Captus thyroid probe used with the adult voxel phantoms: it was placed only proximal to the neck, as for a thyroid count in a clinical setting. Fig. 3 depicts the RFCP with the thyroid probe at the thyroid. Since the sagittal plane passes between the legs of the phantom, only a portion of one leg of the RFCP is intersected by that plane. In addition, the breasts do not appear in this view. In all cases, the positions of the probes proximal to the thyroid are limited by the rigidity of the computational phantoms. During scans of real individuals, the head would be tilted back to allow a closer approach to the neck.

Fig. 4 shows the RMCP facing one of the pillars of the TPM-903B portal monitor. This application differs from the conventional use of this instrument, in which the individual being screened walks between the pillars. The illustration depicts the standard model of the TPM-903B—the extra-wide model is identical except for the wider spacing of the columns.

Other geometries were constructed to simulate exposure rates in air at 16 positions with respect to each phantom: at distances of 2 inches (5.08 cm) and 1, 2, and 3 feet (30.48, 60.96, and 91.44 cm) in the AP and PA orientations in horizontal planes passing through the centers of mass of the stomach and of the lungs. Two additional positions—at distances of 2 inches and 1 foot anterior of the thyroid—were included for assessing intakes of ^{131}I. These exposure geometries constitute a virtual instrument; thus, the analysis comprises the study of four instruments.

MCNP analyses—MCNPX simulations were performed of count rates or exposure rates from each of the four radionuclides distributed in specified DCAL source regions in the seven phantoms, recorded on four instruments. There were separate MCNPX analyses of each region listed in Table 6 for each radionuclide and pathway, as shown in the table. For the Ludlum and Captus instruments, each simulation of the probes positioned at the lungs or the stomach modeled two detectors—one in the AP, the other in the PA orientation, as shown in Figs. 1 and 2. The count rates in each of the two probes were tallied separately. Since each detector was largely shielded by the mass of the phantom from any radiation backscattered from the other detector, there was a negligible effect on the count rates but a significant reduction in labor and computer time. Only those DCAL source regions that are part of the inhalation pathway analysis were included in the simulations of the probes positioned at the lungs, and only the regions for the ingestion analysis were included in those at the stomach. Regions relevant to both pathways were included in the ^{131}I simulations of the probes at the thyroid and in simulations of count rates on the portal monitor and of exposure rates from all four radionuclides. An example of the results is shown in Table 7, which lists normalized count rates on the Ludlum detector from ^{60}Co in the selected source regions of the adult male. The complete set of count rates and exposure rates are listed by Anigstein and Olsher (2016, Appendix C).

MCNP displays the relative error (RE) (i.e., the coefficient of variation) for each mean value in the output file. The RE is based on the Monte Carlo sampling and normally decreases with an increase in the number of simulations, just as the uncertainties in counts on a physical detector decrease with increased counts. MCNPX allows the user to specify a desired RE for a selected tally—the simulations end when the specified RE is achieved. In the present study, a desired RE was specified for each initial simulation, such that the statistical uncertainties of the resulting calibration factors would not exceed ~2%. Since regions that contained smaller fractions of the intake activity have less weight in the calibration factors, less precision was required for the corresponding simulations.

To ensure a comprehensive analysis, all source regions were included that together contained at least 99% of the activity of each of the four radionuclides that is retained in the body at any time from 1 h to 30 d after intake. The analysis comprised 2,646 separate MCNPX simulations, not including runs that were repeated or continued.

Radionuclide emission spectra—The principal source of the decay schemes of radionuclides in the present study was the “WWW Table of Radioactive Isotopes” (TORI) (Chu et al. 1999), which was the basis of the earlier studies reported by Anigstein et al. (2007–2010). Table 8 lists the spectrum of each gamma-emitting radionuclide used in the

present analysis. The L x rays emitted during the decay of ^{192}Ir were omitted from the spectrum of this radionuclide. These x rays, with energies of 8.3–13 keV, constitute 2.5% of the photon intensity but only 0.074% of the energy flux. When emitted from any of the anatomical regions included in the present study, they would be strongly absorbed in the overlying tissues and in the entrance windows of the detectors.

The photon spectra used in this study were compared to the most recent spectral data for these radionuclides. Data on the x-ray spectra of all four radionuclides and on the gamma-ray spectra of ^{131}I and ^{137}Cs were extracted from "ENDF/B-VII.1 Decay Data" (LANL 2012). This database contains detailed listings of the Evaluated Nuclear Structure Data File (ENDSF; BNL 2016) in a readily accessible format that is current as of December 2011. The gamma-ray spectra of ^{131}I and ^{137}Cs were last evaluated in 2006 and 2007, respectively, so these data are current. The gamma ray spectra of ^{60}Co and ^{192}Ir were reevaluated in 2013 and 2012, respectively—these data were extracted directly from the ENDSF. The total energy flux from each radionuclide derived from the spectra used in this study differs by ≤0.25% from the corresponding flux derived from the most recent spectral data. The relative energy fluxes of individual spectral lines, normalized to the total energy flux from the given radionuclide, differ by ≤0.1%. These differences are well within the desired accuracy of the calibration factors derived in this study.

Gaussian energy broadening—The MCNPX simulations of the Model TPM-903B portal monitor employed Gaussian energy broadening, which was applied to the pulse height distribution to account for the energy resolution of the detectors. Part I of the present series presented a more detailed discussion of this MCNP option.

RESULTS

The distributions of activities among selected source regions were combined with the normalized count rates and exposure rates from activities in these regions to develop sets of calibration factors that serve as input data for ICAT.

Energy windows

The Ludlum Model 44-2 is normally used with a rate meter that has no provisions for adjusting the energy discriminator. As discussed in Part I of the present series, an assumed threshold of 1 keV, which is the lowest energy of photons and electrons transported by MCNPX, produced the best match between the MCNPX simulations and experimental measurements—this threshold value was used in deriving calibration factors for this instrument. The Captus 3000 thyroid uptake system and the TPM-903B portal monitor allow the user to specify upper and lower energy limits. The lower energy threshold used in deriving the calibration factors for the Captus 3000 was 10 keV, the lowest value recommended by the manufacturer. The factory setting of the lower-level discriminator (LLD) on early models of the TPM-903B portal monitor was 0.098 V, which corresponds to a photon energy of 32.3 keV, assuming a nominal ratio of 330 keV per volt (TSA 2006). The LLD on current models is set to 0.068 V, which corresponds to 22.4 keV. Two sets of calibration factors, corresponding to these two LLD values, were developed for this instrument.

The upper limit of the energy window in the simulations of count rates on the Ludlum and Captus instruments from each radionuclide was set above the highest photon energy in the corresponding spectrum. The simulations of count rates on the TPM-903B used an upper limit of 1650 keV, which corresponds to the factory setting of the upper-level discriminator of 5.04 V.

Calibration factors

Calibration factors for the three physical instruments are represented by the following expression:

$$F_{gijklptw} = \sum_{m} C_{giklmw} f_{gijmpt}, \quad (1)$$

where

$F_{gijklptw}$ = calibration factor for assessment of individual g (characterized by age of child or gender of adult) at time t following intake of radionuclide i via pathway p (with lung absorption type j for the inhalation pathway), measured with instrument k in position or location l, using energy window w (s^{-1} Bq^{-1});

c_{giklmw} = normalized count rate from radionuclide i in region m of individual g, measured with instrument k in position or location l, using energy window w (s^{-1} Bq^{-1}); and

f_{gijmpt} = fraction of intake activity of radionuclide i (with lung absorption type j for the inhalation pathway) in organ m of individual g at time t after intake via pathway p.[8]

Calibration factors for exposure rates in units of μR h^{-1} Bq^{-1} are represented by a similar expression that is not dependent on energy windows.

An alternate set of calibration factors in units of Bq min was calculated to provide a convenient method of estimating intakes without using ICAT:

$$G_{gijklptw} = \frac{1}{F_{gijklpyw}\kappa}, \quad (2)$$

where

$G_{gijklpwt}$ = alternate calibration factor for assessment of individual g (characterized by age of child or gender of adult) at time t following intake of radionuclide i via pathway p (with lung absorption type j for the inhalation pathway), measured with instrument k in position or location l, using energy window w (Bq min); and

k = temporal conversion factor,

[8] A subset of these normalized activities, calculated for 12 time steps, are tabulated by Anigstein and Olsher (2016, Appendix B).

$= 60\ \text{s min}^{-1}$.

An illustrative example is displayed in Table 9, which lists a set of calibration factors for the Ludlum Model 44-2 at 12 selected time steps after inhalation of Type M and Type S ^{60}Co by an adult male. A complete set of calibration factors for these 12 time steps are tabulated by Anigstein and Loomis (2016, Appendix A), who present a more detailed discussion of the use of these factors for assessing intakes by affected individuals. These time steps are a subset of the 50 time steps in the input data for ICAT.

ICAT computer program

The ICAT computer software package enables a radiation professional to estimate the activity of a gamma-emitting radionuclide taken in by an individual and the cumulative and committed effective dose to that individual.[9] The program can be used under the following conditions:

- there is a single gamma-emitting radionuclide that has been identified;
- the duration of the intake was brief compared to the elapsed time since the intake; and
- the time of intake is known.

The program, which is available for downloading from the CDC website, can be installed on a computer operating under Microsoft Windows XP or higher. ICAT provides two screens for user input and output. The first screen, titled *Client*, illustrated in Fig. 5, is displayed when the program opens. The second screen, titled *Energy Windows*, that is selected by pressing the corresponding tab in the upper left corner of the *Client* screen, is shown in Fig. 6. A third screen, titled *Quick Reference*, displays a condensed reference guide to the operation of the program.

In the example illustrated in Fig. 5, a 20-y-old male, referred to as the “client,” was screened for inhalation of ^{137}Cs using the Ludlum Model 44-2, employing the default energy window of 1–700 keV for this radionuclide and this instrument, 48 h after the suspected intake. A background count rate of 1,500 min^{-1} was recorded on the instrument before the client was brought to the screening location.[10] The probe, coupled to a rate meter, was proximal to his chest in the AP orientation. A gross count rate (client plus background) of 2,000 min^{-1} was recorded.

Having entered the information on the client, the instrument, the date and time of the incident, and the identity and chemical form of the radionuclide, the user pressed the “SI” radio button in the upper right panel to specify that the results be displayed in SI units and then pressed “Calculate Results.” ICAT calculated an intake of 58.4 kBq, a cumulative effective dose of 8.1 μSv that had been delivered up to the time of the program was executed (which might be later than the time of measurement), and a committed effective dose of 270

[9]In the present context, “radiation professional” refers to an individual who has a basic understanding of radiation measurements and has been trained in the proper use of radiation detection instruments. This individual can be a health physicist, a medical physicist, a radiological technologist, a nuclear medicine technologist, a nurse, or another professional with training in radiation detection.
[10]This was the average background count rate measured on this instrument during the study reported in Part I of the present series.

μSv in the absence of medical intervention. All of the data shown on the *Client* screen are saved in a text file on the user's computer that can be accessed by clicking the name of the subdirectory on the local computer that is shown at the bottom left of the screen.

The minimum detectable intake activity (MDIA) in the present example can be calculated by applying the following formula, based on Knoll (2010):

$$\alpha = \frac{4.65\sqrt{bt_c + 2.71}}{F_1 t_c}, \quad (3)$$

where

α = MDIA,

= 35,930 Bq;

b = background count rate,

= 1,500 min^{-1},

= 25 s^{-1};

t_c = effective counting time,

= $2\tau_c$ (Knoll 2010),

τ_c = time constant of detector-rate meter combination (assuming the detector was coupled to a Ludlum Model 16 Analyzer),

= 10.6 s (derived in Part I of the present series); and

F_1 = calibration factor for assessment of adult male, 2 d following inhalation of ^{137}Cs with lung absorption type *F*, measured with a Ludlum Model 44-2 gamma scintillator proximal to the chest in the AP orientation, using the default energy window,

= 1.441×10^{-4} s^{-1} Bq^{-1} (ICAT input data).

The MDIA of 35.9 kBq is significantly less than the calculated intake of 58.4 kBq, which shows that the derived intake activity is statistically significant at the 95% confidence level. Since the calculated committed effective dose of 270 μSv is far below the CDG of 250 mSv for adults, the methodology is sufficiently sensitive to determine if the client exceeded the CDG in the present example.

The next question that arises is: Does the instrument, as used in the present example, have a sufficient range to assess an intake that would result in a committed dose equal to the CDG? Based on the dose coefficient listed by DCAL—4.67×10^{-9} Sv Bq^{-1} for the inhalation of ^{137}Cs with lung absorption type *F* and a particle size distribution of 1 μm AMAD by an adult—a committed effective dose of 250 mSv corresponds to an acute intake of 53.5 MBq. Applying the previously cited calibration factor F_1, the count rate from such an intake is predicted to be 7.714 s^{-1}, excluding background. According to Ludlum Measurements Inc., the dead time for the Ludlum gamma scintillator coupled to a Ludlum Model 16 Analyzer is 10 μs.[11] Assuming the counting system is nonparalyzable, the effect of dead time losses on

the observed count rate can be calculated by the following formula, derived from Knoll (2010):

$$m = \frac{n}{1 + n\tau_d}, \quad (4)$$

where

m = recorded count rate,

= 7,183 s^{-1};

n = true interaction rate,

= calculated count rate + background,

= 7,714 + 25 s^{-1} = 7,739 s^{-1}; and

τ_d = dead time,

= 10^{-5} s.

The relative error due to dead time losses can then be expressed as

$$\delta = \frac{n - m}{n}, \quad (5)$$

where

δ = relative error due to dead time losses,

= 7.2%.

Such an error is well within the accuracy of the model. However, it can be lowered by positioning the probe further from the chest. At a distance of 30.48 cm (1 foot) anterior of the chest, the count rate is reduced to 1,957 s^{-1} (excluding background), and the relative error due to dead time losses is reduced to 2.0%. ICAT allows the user to specify any distance between 0 and 30.48 cm (1 foot) in units of feet, inches, or cm. For intermediate distances, ICAT calculates a new calibration factor, using an algorithm based on the inverse square law to interpolate between the tabulated 0- and 1-foot calibration factors.

The energy windows for each of the three physical instruments can be adjusted using the *Energy Windows* screen. The screen displayed in Fig. 6, that is used to set energy windows on the TPM-903B, presents the user with three sets of discriminator values, which can be selected by pressing the corresponding radio buttons. The default set, which is fixed, comprises the factory settings on current models of this instrument. The alternate set, which is also fixed, contains the factory settings on an early version of this monitor. Selecting the custom set enables the user to edit and save a new set of discriminator values. ICAT converts

[11]Ludlum Measurements Inc., 17 December 2015, personal email to Robert Anigstein.

these values to energy windows, using the nominal ratio of 330 keV per volt, and applies these windows to the stored count rates (tabulated in 1-keV-wide energy bins) to calculate a new set of normalized count rates. The program then applies eqn (1) to calculate a new set of calibration factors. Custom windows, with upper and lower threshold energies expressed in units of keV, can also be specified for the Ludlum and the Captus detectors—ICAT calculates new calibration factors corresponding to these windows.

If the elapsed time from intake to assessment falls between the 50 tabulated values, ICAT calculates a new calibration factor by linear interpolation of the calibration factors for adjacent times. ICAT also derives a new calibration factor if the client's age falls between the ages of the reference individuals, deriving a new activity distribution among the source regions by linear interpolation of the activity distributions in reference individuals of adjacent ages. If the client is less than 15 y old, and if the client's weight[12] (an optional entry for clients age <15 y) is specified, ICAT calculates new normalized count rates from each source region by linear interpolation of count rates from reference individuals whose masses bracket the mass of the client.

DISCUSSION

The calibration factors derived in the present study are dependent on the biokinetic models embodied in the DCAL computer code and on the MCNP models of the revised ORNL pediatric phantoms and of the voxel phantoms described by ICRP (2009). These models were developed to determine radiation protection standards for the general population and are based on the anatomy and physiology of reference individuals—they do not necessarily reflect the anatomy and physiology of any given individual.

These calibration factors were derived during the development of the ICAT computer program. The factors were calculated using MCNP models of the instruments that had been previously validated by comparing the MCNPX simulations to experimental measurements. During the study reported in Part I of the present series, the simulations were revised to use newer radioactive decay data, more detailed MCNP techniques, and some updated models of the instruments, resulting in better agreement between the measured and calculated values.

One such revision involved the MCNPX simulations of count rates from ^{60}Co and ^{137}Cs. In simulating count rates on scintillation detectors from gamma-emitting radionuclides, MCNP is typically operated in mode *p*, in which only the transport of photons is modeled explicitly. In this mode, the kerma generated by secondary electrons is deposited at the collision site.[13] However, photons produced by these particles following ionization, bremsstrahlung, or annihilation are transported, although the initial location, direction, and energy are slightly different than they would be if the secondary particle had been transported.[14] Mode *p* allows the code to execute more efficiently and is sufficiently accurate for most purposes. However, the high-energy gamma rays emitted by ^{60}Co can produce high-energy electrons by

[12]ICAT uses the term "weight," which is likely to be more familiar to field workers, instead of the scientific term "mass" used by ICRP (2002).
[13]In the present discussion, the term "electrons" also encompasses positrons. In MCNP, "positron physics is identical to electron physics, except for positron annihilation [Pelowitz 2011]."
[14]John S. Hendricks, 19 May 2016, personal email to Robert Anigstein.

Compton scattering and, to a lesser extent, by pair production. These electrons can have a sufficiently long range to affect the MCNP simulations of counts recorded on the detector. Modeling the transport of both electrons and photons (mode *p e* in MCNP terminology) explicitly accounts for this effect and can yield more accurate results. Mode *p e* was used in the MCNPX simulations of ^{60}Co and ^{137}Cs reported in Part I; however, using this mode in the derivation of calibration factors for these radionuclides would have required much longer execution times, which would have significantly prolonged the analyses, given the large number of simulations required.

In order to estimate the impact of using mode *p*, a new set of 200 calibration factors for the inhalation of both Type *M* and Type *S* ^{60}Co at 50 time steps were derived from a set of MCNPX simulations using mode *p e*. These simulations modeled count rates on the Ludlum Model 44-2 scintillation probe proximal to the chest of an adult male in both the AP and PA orientations. Except for the different mode, the new simulations used the same parameters as before. The new calibration factors were 0.2–2.3% higher than the old ones. Since ^{137}Cs emits gamma rays of much lower energy, the effect for this radionuclide would be much smaller, as confirmed by an unpublished study that showed no statistically significant differences between mode *p* and mode *p e* in simulating count rates from ^{137}Cs on an NaI(Tl) scintillation detector.

The MCNP models of the Ludlum Model 44-2 scintillation probe and the Captus 3000 thyroid probe used in the study reported in Part I of the present series had been updated to more closely conform to the manufacturers' descriptions of these instruments and their components. To estimate the impact of the first of the revised models, new calibration factors were derived from MCNPX simulations of count rates on the Ludlum probe proximal to the abdomen of an adult female in both the AP and PA orientations following ingestion of ^{192}Ir using the updated model of this instrument. These simulations used the updated ^{192}Ir photon spectrum, described previously. There were no statistically significant differences between calibration factors derived from these simulations and the old factors. New MCNPX simulations were also performed of count rates on the Captus 3000 thyroid probe proximal to the thyroid of an adult male following inhalation of ^{131}I to estimate the impact of the revised model of this instrument. Calibration factors derived from these results were ~2.1% higher than the original values.

Finally, a new set of MCNPX simulations of count rates on the TPM-903B portal monitor following the ingestion of ^{137}Cs by an adult female were performed in order to estimate the impact of a simplified Gaussian energy broadening method as well as the updated photon spectrum for this radionuclide. There were no statistically significant differences between calibration factors derived from these results and the original factors.

These analyses show that differences between the original and recalculated sets of calibration factors are comparable to the statistical uncertainties of these factors. It is therefore concluded that the validation of the MCNP models and methods used to simulate count rates on three physical instruments, reported in Part I of the present series, remains applicable to the study reported in the present paper.

While the present study is limited to four gamma-emitting radionuclides, intakes of some beta-emitting radionuclides can also be estimated by in vivo bioassay. A notable example is ^{90}Sr, mentioned earlier in this paper. Except for freshly separated material, this radionuclide is in secular equilibrium with its short-lived progeny, ^{90}Y ($t_{½}$ = 64 h), that emits beta rays with a maximum energy of 2.28 MeV. Although ^{90}Sr is a pure beta emitter and ^{90}Yemits beta rays and very low intensity x and gamma rays, following an intake of these radionuclides, the high-energy ^{90}Y beta rays would generate bremsstrahlung x rays that could be measured by sufficiently sensitive radiation detection instruments. As previously mentioned, Anigstein et al. (2007–2010) developed calibration factors that enable nuclear medicine gamma cameras to be used for estimating intakes of ^{90}Sr in secular equilibrium with ^{90}Y.

CONCLUSION

The tables of calibration factors described in the present paper and the ICAT computer software package that uses these factors constitute convenient screening tools for use after a radiological incident that results in acute intakes of one of four gamma-emitting radionuclides—^{60}Co, ^{131}I, ^{137}Cs, and ^{192}Ir—by inhalation or ingestion. When there is a potential for a large population to be internally contaminated with one of these radionuclides, these screening tools can be useful for the rapid triage of those individuals and for setting priorities for more definitive assessments.

Acknowledgments

The authors gratefully acknowledge the support and assistance of Keith Eckerman, Oak Ridge National Laboratory, who provided advice and information on the use of the DCAL software system; and of Wesley Bolch, Professor of Radiological and Biomedical Engineering at the University of Florida, who provided the MCNP models of the revised ORNL phantom series.

This work was supported by Contract No. GS-10F-0093K from the Centers for Disease Control and Prevention (CDC) with S. Cohen & Associates (SC&A, Inc.). Additional support was provided by SciMetrika, LLC, under Contract No. 200-2009-28540, Task Order 0008. The findings and conclusions in this report are those of the authors and do not necessarily represent the official position of the Centers for Disease Control and Prevention/the Agency for Toxic Substances and Disease Registry.

References

Anigstein R, Erdman MC, Ansari A. Use of transportable radiation detection instruments to assess internal contamination from intakes of radionuclides. Part 1: field tests and Monte Carlo simulations. Health Phys. 2016; 110:612–622. DOI: 10.1097/HP.0000000000000496 [PubMed: 27115229]

Anigstein, R., Loomis, DA. [Accessed 6 July 2016] Use of transportable radiation detection instruments to assess internal contamination from intakes of radionuclides. Part 4: instructions for users [online]. 2016. Available at https://emergency.cdc.gov/radiation/clinicians/evaluation/pdf/field_instruments_iv.pdf

Anigstein, R., Loomis, DA., Olsher, RH. [Accessed 22 May 2016] Assess: a program to help hospital staff use gamma cameras to assess accidental intakes of radioisotopes [computer software, online]. 2009. Available at https://emergency.cdc.gov/radiation/clinicians/evaluation/zips/ASSESSv_1_2_10.zip

Anigstein, R., Loomis, DA., Olsher, RH. [Accessed 3 March 2016] ICAT (Internal Contamination Assessment Tool): a program to help radiation professionals use radiation measuring instruments to

assess acute intakes of radionuclides [computer software, online]. 2014. Available at https://emergency.cdc.gov/radiation/clinicians/evaluation/zips/ICAT_Version1_1_7.zip

Anigstein, R., Olsher, RH. [Accessed 6 July 2016] Use of transportable radiation detection instruments to assess internal contamination from intakes of radionuclides. Part 3: supplementary data [online]. 2016. Available at https://emergency.cdc.gov/radiation/clinicians/evaluation/pdf/field_instruments_iii.pdf

Anigstein, R., Olsher, RH., Erdman, MC., Engdahl, JC. [Accessed 6 July 2016] Use of radiation detection, measuring, and imaging instruments to assess internal contamination from intakes of radionuclides. Parts 2–5 [online]. 2007–2010. Available at http://emergency.cdc.gov/radiation/clinicians/evaluation/supportdocs.htm

Argonne National Laboratory, Environmental Science Division. [Accessed 9 May 2015] Human health fact sheet, August 2005: radiological dispersal device (RDD); Radiological and chemical fact sheets to support health risk analyses for contaminated areas [online]. 2007. p. 80-85.[unnumbered in PDF file]. Available at www.remm.nlm.gov/ANLContaminantFactSheetsAll070418.pdf

Behling, UH., Hildebrand, JE. [Accessed 8 July 2016] Radiation and health effects: a report on the TMI-2 accident and related health studies. GPU Nuclear Corporation [online]. 1986. Available at www.threemileisland.org/downloads/224.pdf

Bolch WE, Hurtado JL, Lee C, Manger RP, Burgett EA, Hertel NE, Dickerson W. Guidance on the use of handheld survey meters for radiological triage: time-dependent detector count rates corresponding to 50, 250, and 500 mSv effective dose for adult males and adult females. Health Phys. 2012; 102:305–325. DOI: 10.1097/HP.0b013e3182351660 [PubMed: 22420020]

Brookhaven National Laboratory, National Nuclear Data Center. [Accessed 9 July 2016] Evaluated Nuclear Structure Data File (ENSDF) [online]. 2016. Available at www.nndc.bnl.gov/ensdf/

Chu, SYF., Ekström, LP., Firestone, RB. [Accessed 7 February 2016] WWW table of radioactive isotopes, database version 1999-02-28 [online]. 1999. Available at http://nucleardata.nuclear.lu.se/toi/nucSearch.asp

Dewji S, Hertel N, Ansari A. Assessing internal contamination after the detonation of a radiological dispersion device using a 2×2-inch sodium iodide detector. Radiat Prot Dosimetry. 2013; 155:300–316. DOI: 10.1093/RPD/NCT014 [PubMed: 23436621]

Dimbylow PJ. Induced current densities from low-frequency magnetic fields in a 2 mm resolution, anatomically realistic model of the body. Phys Med Biol. 1998; 43:221–230. doi:ORG/10.1088/0031-9155/43/2/001. [PubMed: 9509522]

Dimbylow PJ. Development of the female voxel phantom, NA-OMI, and its application to calculations of induced current densities and electric fields from applied low frequency magnetic and electric fields. Phys Med Biol. 2005; 50:1047–1070. doi:ORG/10.1088/0031-9155/50/6/002. [PubMed: 15798308]

DOE/NRC Interagency Working Group on Radiological Dispersal Devices. [Accessed 8 July 2016] Radiological dispersal devices: an initial study to identify radioactive materials of greatest concern and approaches to their tracking, tagging, and disposition [online]. 2003. Available at www.energy.gov/sites/prod/files/edg/media/RDDRPTF14MAYa.pdf

Eckerman, KF., Cristy, M., Ryman, JC. [Accessed 21 October 2005] The ORNL mathematical phantom series. 1996. Previously available at https://www.epa.gov/sites/production/files/2015-05/documents/402-r-99-001.pdf

Eckerman, KF., Legget, RW., Cristy, M., Nelson, CB., Ryman, JC., Sjoreen, AL., Ward, RC. [Accessed 7 February 2016] User's guide to the DCAL system, ORNL/TM-2001/190 [online]. 2006. Available at https://www.epa.gov/sites/production/files/2015-02/documents/dcal-manual.pdf

Eckerman, KF., Leggett, RW., Nelson, CB., Puskin, JS., Richardson, ACB. [Accessed 13 July 2016] Cancer risk coefficients for environmental exposure to radionuclides. Federal Guidance Report No. 13, EPA-402/R-99-001 [online]. 1999. Available at https://www.epa.gov/sites/production/files/2015-05/documents/402-r-99-001.pdf

Han EY, Bolch WE, Eckerman KF. Revisions to the ORNL series of adult and pediatric computational phantoms for use with the MIRD schema. Health Phys. 2006; 90:337–356. doi:ORG/10.1097/01.HP.0000192318.13190.C4. [PubMed: 16538139]

Harper FT, Musolino SV, Wente WB. Realistic radiological dispersal device hazard boundaries and ramifications for early consequence management decisions. Health Phys. 2007; 93:1–16. doi:ORG/10.1097/01.HP.0000264935.29396.6F. [PubMed: 17563488]

Hurtado JL, Lee C, Lodwick D, Geode T, Williams JL, Bolch WE. Hybrid computational phantoms representing the reference adult male and adult female: construction and applications to retrospective dosimetry. Health Phys. 2012; 102:292–304. doi:ORG/10.1097/HP.0B013E318235163F. [PubMed: 22315022]

International Commission on Radiological Protection. ICRP Publication 66; Ann ICRP. Vol. 24. Tarrytown, NY: Elsevier Science, Inc; 1994. Human respiratory tract model for radiological protection.

International Commission on Radiological Protection. ICRP Publication 72; Ann ICRP. Vol. 26. Tarrytown, NY: Elsevier Science, Inc; 1996. Age-dependent doses to the members of the public from intake of radionuclides. Part 5: compilation of ingestion and inhalation coefficients.

International Commission on Radiological Protection. ICRP Publication 89; Ann ICRP. Vol. 32. Oxford: Pergamon Press; 2002. Basic anatomical and physiological data for use in radiation protection: reference values.

International Commission on Radiological Protection. ICRP Publication 110; Ann ICRP. Vol. 39. Tarrytown, NY: Elsevier Ltd; 2009. Adult reference computational phantoms.

International Commission on Radiological Protection. Compendium of dose coefficients based on ICRP Publication 60 [online]. ICRP Publication 119; Ann ICRP. 2012; 41(Suppl) [Accessed 5 February 2016] Available at www.icrp.org/docs/P%20119%20JAICRP%2041%28s%29%20Compendium%20of%20Dose%20Coefficients%20based%20on%20ICRP%20Publication%2060.pdf.

Knoll, GF. Radiation detection and measurement. 4. New York: John Wiley & Sons, Inc; 2010.

Kramer GH, Capello K, Hauck BM. The HML's new field deployable, high-resolution whole body counter. Health Phys. 2005; 89(Suppl 5):S60–S68. doi:ORG/10.1097/01.HP.0000178537.20710.42. [PubMed: 16224263]

Kramer GH, Noel L, Burns LC. The BRMD BOMAB family. Health Phys. 1991; 61:895–902. doi:ORG/10.1097/00004032-199112000-00025. [PubMed: 1955336]

Los Alamos National Laboratory. [Accessed 9 May 2015] ENDF/B-VII.1 decay data [online]. 2012. Available at http://t2.lanl.gov/nis/data/endf/decayVII.1.html

Manger RP, Hertel NE, Burgett EA, Ansari A. Using handheld plastic scintillator detectors to triage individuals exposed to a radiological dispersal device. Radiat Prot Dosimetry. 2012; 150:101–108. DOI: 10.1093/RPD/NCR367 [PubMed: 22128361]

National Council on Radiation Protection and Measurements. Management of persons contaminated with radionuclides: handbook. Bethesda, MD: NCRP; 2008. Report No. 161

Oak Ridge National Laboratory, Life Science Division, Dosimetry Research Group. [Accessed 22 October 2016] DCAL: dose and risk calculation system, ver. 8.4. [computer software and manual, online]. 2006. Ver. 9.5 available at https://www.epa.gov/sites/production/files/2016-10/dcalsetup_0.exe

Palmer RC, Hertel NE, Ansari A, Manger RP, Freibert EJ. Evaluation of internal contamination levels after a radiological dispersal device incident using portal monitors. Radiat Prot Dosimetry. 2012; 151:237–251. DOI: 10.1093/RPD/NCS006 [PubMed: 22332142]

Pelowitz, DB. MCNPX user's manual version 2.7.0, LA-CP-11-00438. Los Alamos National Laboratory. MCNP5/MCNPX: Monte Carlo N-Particle transport code system including MCNP5-1.60 and MCNPX 2.7.0 and data libraries, RSICC Code Package CCC-740 [computer software and manual]. Oak Ridge, TN: Oak Ridge National Laboratory; 2011. [CD-ROM]

TSA Systems, Ltd. [Accessed 7 May 2015] Transportable portal monitor model TPM-903B: operating and service manual, Doc. #5003 Rev. A [online]. 2006. Available at www.laurussystems.com/Service/TPM-903BUser-Guide092009.pdf

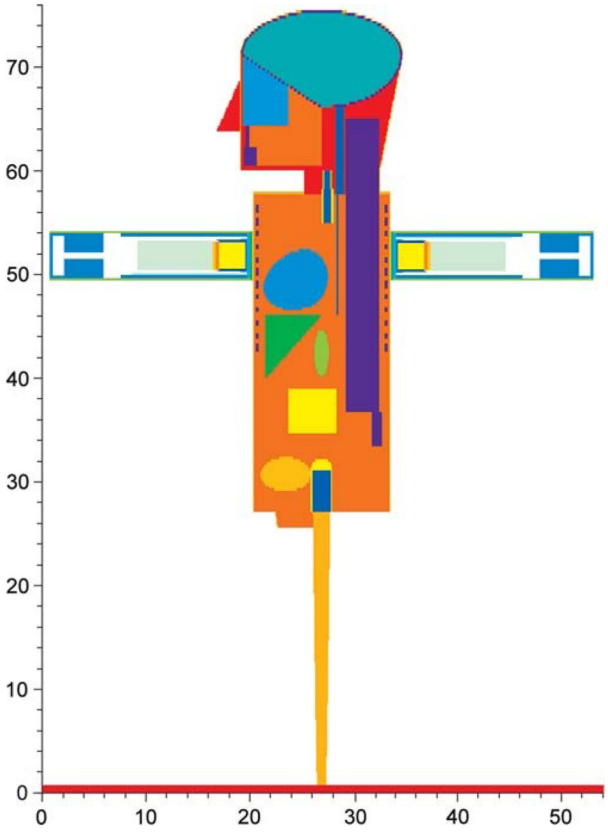

Fig. 1.
Cross-section of 1-y-old with Ludlum Model 44-2 detectors proximal to lungs (scale in cm).

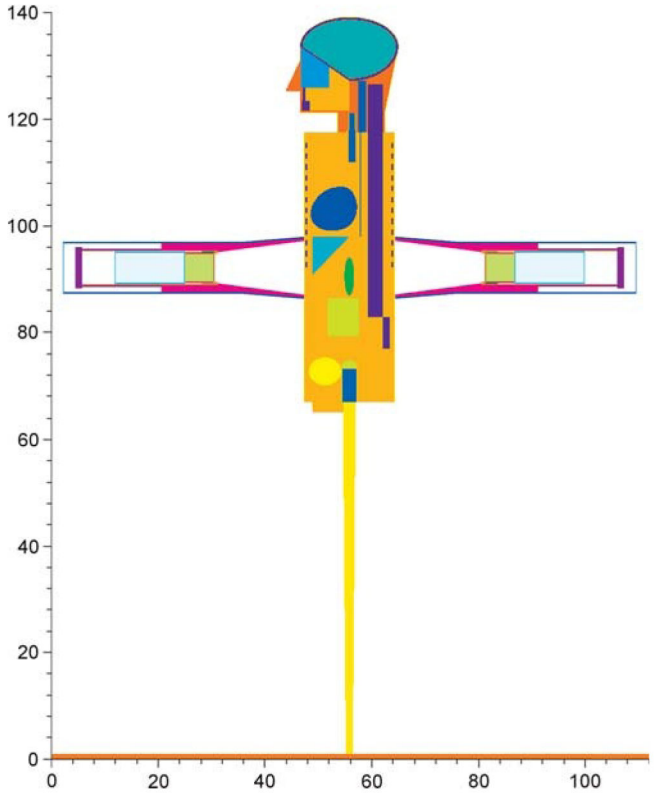

Fig. 2.
Cross-section of 10-y-old with Captus 3000 thyroid probes proximal to stomach (scale in cm).

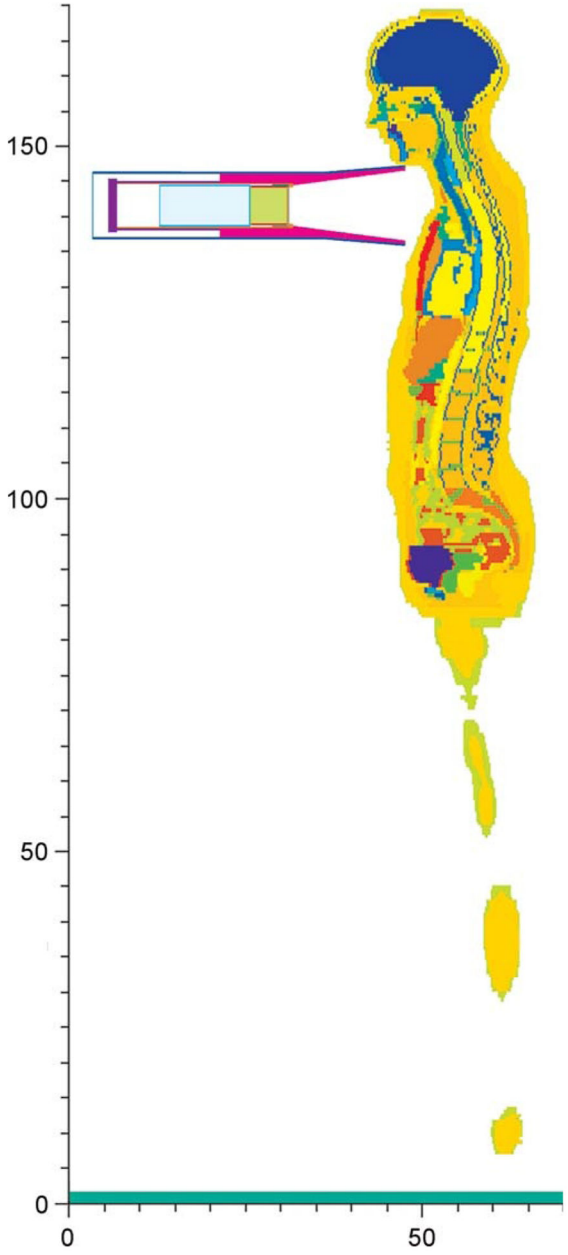

Fig. 3.
Cross-section of RFCP with Captus 3000 thyroid probe proximal to thyroid (scale in cm).

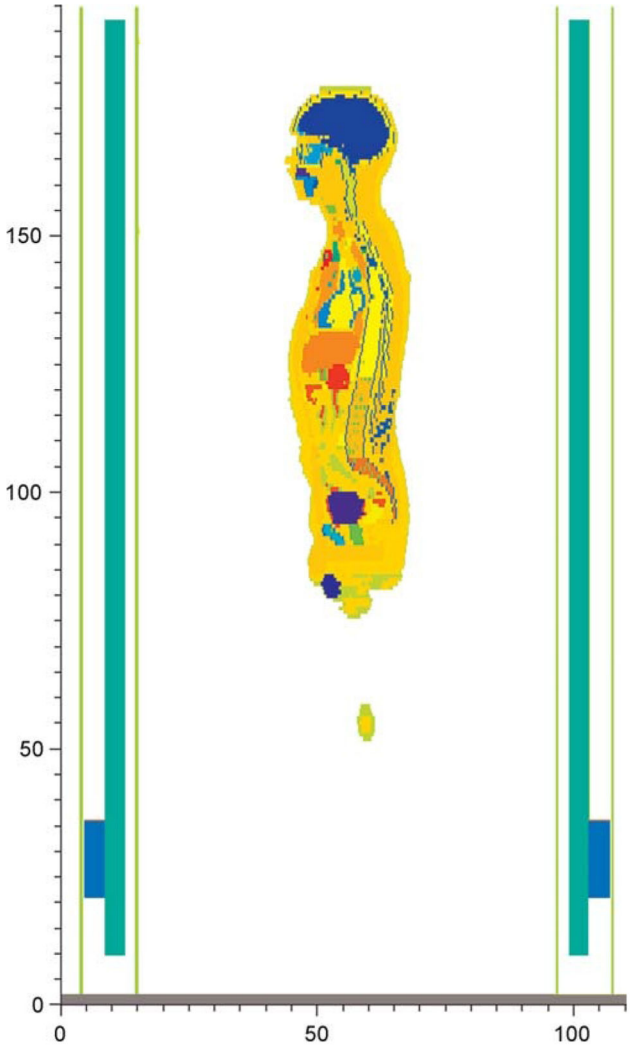

Fig. 4.
Cross-section of RMCP with TPM-903B portal monitor (standard width) (scale in cm).

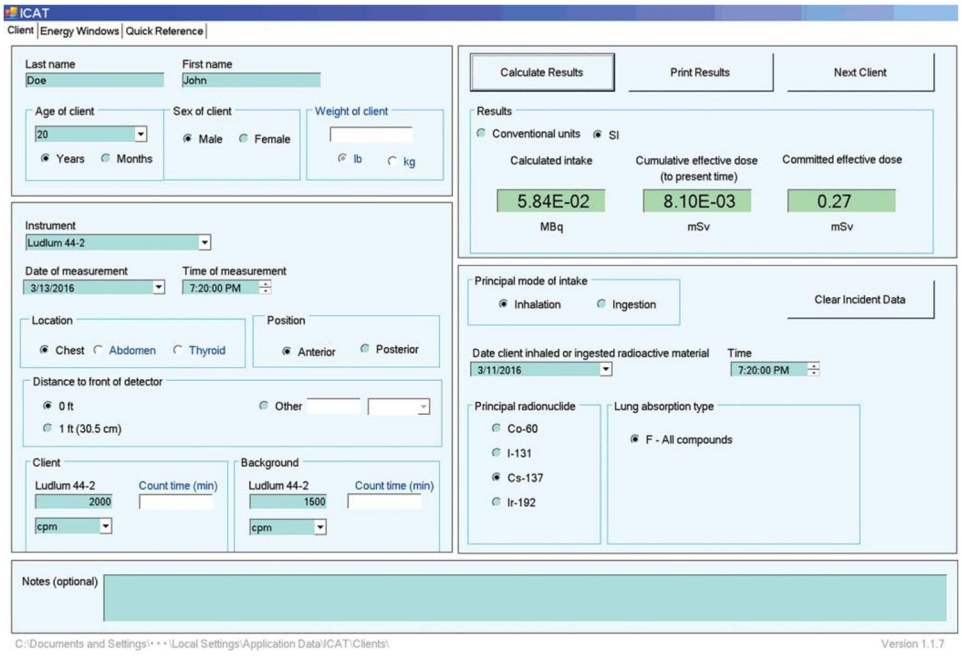

Fig. 5.
Example of *Client* screen displayed by ICAT computer code.

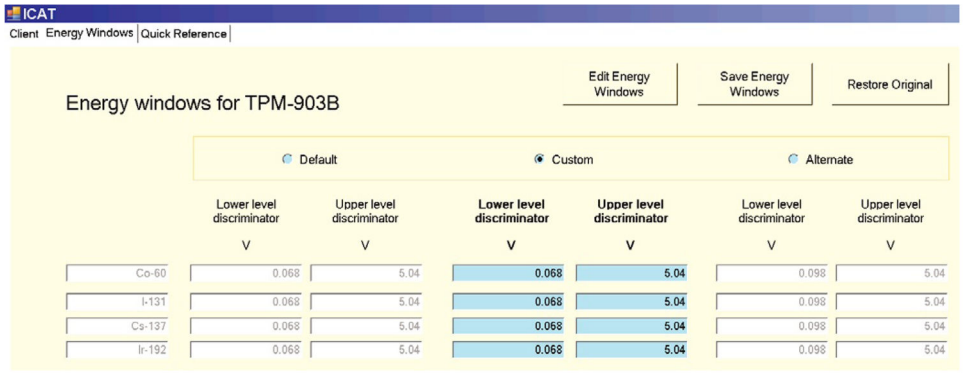

Fig. 6.
Example of *Energy Windows* screen displayed by ICAT computer code.

Table 1

Lung absorption types.[a]

Element	Lung type	Chemical forms
Co	M	Unspecified compounds
	S	Oxides, hydroxides, halides, and nitrates
I	F	All compounds
Cs	F	All compounds
Ir	F	Unspecified compounds
	M	Metallic iridium, halides, and nitrates
	S	Oxides and hydroxides

[a]Source: ICRP 2012, Table E.1.

Table 2

f_1 values used in DCAL calculations.

			Age		
Element	**Pathway**	**Lung type**	**Infant**	**1–15 y**	**Adult**
Co	Ingestion		0.6	0.3	0.1
	Inhalation	M	0.2	0.1	0.1
		S	0.02	0.01	0.01
I	Ingestion		1	1	1
	Inhalation	F	1	1	1
Cs	Ingestion		1	1	1
	Inhalation	F	1	1	1
Ir	Ingestion		0.02	0.01	0.01
	Inhalation	All	0.02	0.01	0.01

Health Phys. Author manuscript; available in PMC 2017 November 28.

Table 3

Names and descriptions of selected DCAL source regions.

Name	Description[a]
AI	Alveolar interstitial tissue
bbe-gel	Mucous (gel) layer of bronchiolar airways
bbe-sol	Sol layer of bronchiolar airways
bbe-seq	Macrophages in bronchiolar lamina propria that sequester particles
BBi-gel	Mucous (gel) layer of bronchial airways
BBi-sol	Sol layer of bronchial airways
BBi-seq	Macrophages in bronchial lamina propria that sequester particles
ET1	Anterior nose (ET_1)
St_Cont	Stomach contents
SI	Small intestine contents
ULI_Cont	Upper large intestine contents
LLI_Cont	Lower large intestine contents

[a]Names based on the ICRP model of the human respiratory tract (ICRP 1994).

Table 4

Anatomical regions of revised ORNL pediatric phantoms corresponding to DCAL source regions.

	Revised ORNL pediatric phantom[a]					
Anatomical region	**Infant**	**1 y**	**5 y**	**10 y**	**15 y**	**DCAL source regions[b]**
Bronchial mucosa	—	—	—	—	—	BBi-gel BBi-sol BBi-seq AI
Lung-left	46.3%	46.5%	46.3%	46.3%	46.4%	bbe-gel
Lung-right	53.7%	53.5%	53.7%	53.7%	53.6%	bbe-sol bbe-seq
Nose contents	—	—	—	—	—	ET1
Ascending colon contents	43.0%	43.8%	43.3%	43.5%	43.3%	ULI_Cont
Proximal transverse colon contents	28.5%	28.1%	28.4%	28.3%	28.3%	
Distal transverse colon contents	28.5%	28.1%	28.4%	28.3%	28.3%	
Descending colon contents	45.2%	44.1%	45.1%	45.4%	44.9%	LLI_Cont
Sigmoid colon contents	54.8%	55.9%	54.9%	54.6%	55.1%	
Left kidney	50%	50%	50%	50%	50%	Kidneys
Right kidney	50%	50%	50%	50%	50%	

[a] Percentage of DCAL source region(s) represented by each phantom region, based on relative mass of each phantom region.

[b] See Table 3.

Table 5

Anatomical regions of voxel phantoms corresponding to DCAL source regions.

Voxel regions	RMCP[a]	RFCP[a]	DCAL source regions[b]
Trachea	13.1%	47.9%	BBi-gel BBi-sol
Bronchi	86.9%	52.1%	BBi-seq
Lung, left, tissue	45.2%	44.4%	AI bbe-gel bbe-sol
Lung, right, tissue	54.8%	55.6%	bbe-seq
Ascending colon contents	29.0%	52.6%	ULI_Cont
Transverse colon contents, right	50.0%	31.6%	
Transverse colon contents, left	21.1%	15.8%	
Descending colon contents	31.8%	38.5%	LLI_Cont
Sigmoid colon contents	68.2%	61.5%	
Kidney, left, cortex	34.6%	38.0%	Kidneys
Kidney, left, medulla	12.3%	13.6%	
Kidney, left, pelvis	2.5%	2.7%	
Kidney, right, cortex	35.5%	32.0%	
Kidney, right, medulla	12.7%	11.4%	
Kidney, right, pelvis	2.5%	2.3%	

[a]Percentage of DCAL source region represented by each voxel region, based on relative mass of each region in the RMCP and RFCP.

[b]See Table 3.

Table 6

DCAL source regions included in MCNPX simulations.[a]

	Radionuclide/pathway(s)			
DCAL source region	**^{60}Co**	**^{131}I**	**^{137}Cs**	**^{192}Ir**
Lung	H			H
Bronchial airways	H			H
Surface of anterior nasal passage (ET_1 in ICRP 1994)	H	H	H	H
Stomach contents	G,H	G,H	G,H	G,H
Small intestine contents	G,H	G	G	G,H
Blood	G,H	G,H	G,H	G,H
Upper large intestine contents	G,H			G,H
Lower large intestine contents	G,H	G		G,H
Other: all tissues not specified in biokinetic model of given element	G,H	G,H		G,H
Body tissues: similar to Other, but excludes mineralized bone			G,H	
Kidneys				G,H
Spleen				G,H
Liver	G,H			G,H
Thyroid		G,H		
Contents of urinary bladder		G,H		

[a]Note: *G* designates regions utilized in analysis of ingestion pathway, *H* designates inhalation.

Table 7

Normalized count rates on Ludlum Model 44-2 detector from ^{60}Co in selected DCAL source regions of adult male (s^{-1} Bq^{-1}).

	Detector location/distance from body							
	Chest				Abdomen			
	Contact		1 foot		Contact		1 foot	
Anatomical region[a]	Anterior	Posterior	Anterior	Posterior	Anterior	Posterior	Anterior	Posterior
Lung	3.38×10^{-3}	2.88×10^{-3}	3.68×10^{-4}	3.51×10^{-4}	—	—	—	—
BBi	4.51×10^{-3}	2.35×10^{-3}	4.00×10^{-4}	3.39×10^{-4}	—	—	—	—
ET1	6.78×10^{-4}	1.92×10^{-4}	3.07×10^{-4}	9.65×10^{-5}	—	—	—	—
Stomach	2.78×10^{-3}	1.49×10^{-3}	4.31×10^{-4}	2.87×10^{-4}	3.97×10^{-3}	2.19×10^{-3}	4.17×10^{-4}	3.19×10^{-4}
SI	1.10×10^{-3}	7.80×10^{-4}	3.35×10^{-4}	2.73×10^{-4}	2.29×10^{-3}	1.90×10^{-3}	3.64×10^{-4}	3.42×10^{-4}
Blood	1.93×10^{-3}	1.45×10^{-3}	2.85×10^{-4}	2.64×10^{-4}	1.49×10^{-3}	1.65×10^{-3}	2.81×10^{-4}	2.99×10^{-4}
ULI	1.19×10^{-3}	6.27×10^{-4}	3.82×10^{-4}	2.21×10^{-4}	3.25×10^{-3}	1.40×10^{-3}	4.19×10^{-4}	2.65×10^{-4}
LLI	5.31×10^{-4}	4.51×10^{-4}	2.52×10^{-4}	2.19×10^{-4}	9.50×10^{-4}	9.36×10^{-4}	2.92×10^{-4}	2.70×10^{-4}
Other	7.49×10^{-4}	7.80×10^{-4}	1.81×10^{-4}	2.04×10^{-4}	6.76×10^{-4}	9.19×10^{-4}	1.85×10^{-4}	2.28×10^{-4}
Liver	2.69×10^{-3}	1.64×10^{-3}	4.13×10^{-4}	3.16×10^{-4}	3.75×10^{-3}	2.63×10^{-3}	3.82×10^{-4}	3.56×10^{-4}

[a] See Table 3.

Table 8

Photon spectra of radionuclides (Source: Chu et al. 1999).[a]

^{60}Co		^{131}I		^{137}Cs		^{192}Ir	
E (keV)	**I (%)**	**E (keV)**	**I (%)**	**E (keV)**	**I (%)**	**E (keV)**	**I (%)**
346.93	0.0076	29.11	0.00014	3.95	0.0143	60.90	0.00106
826.06	0.0076	29.46	1.40	4.33	0.0064	61.49	1.20
1,173.24	99.97	29.78	2.59	4.45	0.04	63	2.07
1,332.50	99.99	33.56	0.238	4.47	0.36	64.51	0.00286
Total[b]	199.97	33.62	0.459	4.83	0.226	65.12	2.65
		33.88	0.00467	4.85	0.023	66.83	4.53
		34.42	0.139	4.93	0.039	71.08	0.239
		34.50	0.0269	4.99	0.003	71.41	0.46
		80.18	2.623	5.16	0.074	71.88	0.0113
		85.9	0.00009	5.53	0.033	73.36	0.162
		177.21	0.270	5.80	0.0065	73.59	0.0188
		232.18	0.00319	5.81	0.0093	75.37	0.533
		272.50	0.0578	31.45	0.000263	75.75	1.029
		284.30	6.136	31.82	2.04	76.23	0.0265
		295.8	0.0018	32.19	3.76	77.83	0.365
		302.4	0.00474	36.30	0.352	78.07	0.0478
		318.09	0.0776	36.38	0.68	110.09	0.0126
		324.65	0.0212	36.65	0.0079	136.34	0.183
		325.79	0.274	37.26	0.215	176.98	0.0043
		358.4	0.0163	37.35	0.0481	201.31	0.472
		364.49	81.7	283.53	0.00058	205.80	3.30
		404.81	0.0547	661.66	85.1	280.04	0.023
		503.00	0.360	Total	93.038	283.27	0.262
		636.99	7.173			295.96	28.67
		642.72	0.217			308.46	30.00
		722.91	1.773			316.51	82.81
		Total	105.62			329.31	0.0186

^{60}Co		^{131}I		^{137}Cs		^{192}Ir	
E (keV)	I (%)	E (keV)	I (%)	E (keV)	I (%)	E (keV)	I (%)
						374.49	0.721
						416.47	0.664
						420.53	0.0737
						468.07	47.83
						484.58	3.185
						485.3	0.0022
						489.04	0.443
						588.58	4.515
						593.37	0.0426
						599.4	0.0039
						604.41	8.23
						612.47	5.309
						703.98	0.0053
						766	0.00149
						884.54	0.2923
						1,061.48	0.0528
						1,089.7	0.00108
						1,378.3	0.00124
						Total	230.48

[a] Values used in MCNPX analyses—some values are rounded. Listed precision may exceed precision of adopted values.

[b] Total does not equal the sum of the listed values due to rounding.

Table 9

Inhaled activity of ^{60}Co by adult male vs. count rate on Ludlum 44-2 detector (Bq min).

Time post intake		Lung absorption type/distance of detector from chest/aspect							
		Type *M*				Type *S*			
		Contact		1 foot		Contact		1 foot	
d	h	Anterior	Posterior	Anterior	Posterior	Anterior	Posterior	Anterior	Posterior
	1	17.7	26.3	98.8	144	17.3	25.6	97.5	130
	2	19.7	28.3	103	147	19.3	27.6	101	136
	4	21.2	30.1	106	154	20.9	29.5	104	142
	8	22.6	31.8	113	164	22.2	31.2	110	151
	12	24.1	33.3	123	173	23.5	32.5	119	158
1	24	28.7	37.4	158	204	27.5	35.9	151	185
2		35.3	43.5	237	274	33.3	41.0	227	245
4		40.7	48.8	340	362	37.7	45.4	327	320
8		44.1	52.7	389	407	39.8	47.7	365	350
10		45.4	54.2	401	420	40.6	48.6	372	356
20		52.0	61.8	460	481	44.1	52.7	405	387
30		58.6	69.4	517	540	47.5	56.5	435	416